RSC Sustainability

ROYAL SOCIETY OF CHEMISTRY

PAPER

View Article Online
View Journal

Cite this: DOI: 10.1039/d6su00101g

Mechanochemically engineered ammonium magnesium-sulfate double salts synthesized from ammonium carbonate for improved nitrogen-use efficiency

Mohamed Ammar,†[a] Julia Farias,†[bc] Emmanuel Aransiola,[a] Matthew Conley,[d] Kerry A. Hamilton,[bc] Clinton Williams[d] and Jonas Baltrusaitis *[a]

Ammonium carbonate (AC) represents a concentrated ammonium precursor with potential relevance for nitrogen (N) recovery from anaerobic digestate, but its direct use in soils is limited by chemical instability and rapid N loss. In this study, ammonium carbonate was used as a model ammonium source to synthesize a magnesium ammonium sulfate double salt, $Mg(NH_4)_2(SO_4)_2 \cdot 6H_2O$ (MgSA), and its performance in soil was evaluated relative to ammonium carbonate and urea. In particular, MgSA was prepared *via* a solid-state green solvent-free mechanochemical method and structurally characterized by X-ray diffraction and thermal analysis. MgSA was synthesized at high conversion for the molar $MgSO_4 \cdot 7H_2O$: AC of 0.8 : 1.2 to 1.2 : 0.8 using epsomite salt as a precursor on a mg scale, while 20 gram batches were synthesized using anhydrous $MgSO_4 \cdot 7H_2O$ and AC mixtures. Ammonia volatilization of MgSA was assessed under controlled laboratory conditions, while agronomic performance was evaluated in growth-chamber experiments using romaine lettuce grown in three sandy loam soils with contrasting physicochemical properties. Under high relative humidity, MgSA granules exhibited a significant decrease in NH_3 emission as obtained using the Richards kinetic model, as compared to the AC. In growth chamber experiments, MgSA sustained strong lettuce growth, often matching or exceeding the performance of urea and ammonium carbonate while avoiding excessive soil nitrate accumulation *via* sustained nitrogen delivery, allowing plant uptake to remain stable. The simultaneous supply of magnesium and sulfur enabled chlorophyll synthesis and nitrogen assimilation, demonstrating the value of integrating multiple essential nutrients into a single crystalline phase. We conclude that this work charts pathways for using waste-derived AC as a promising green chemistry agent that can be mechanochemically combined with mineral salts and contribute to global nitrogen cycling.

Received 16th February 2026
Accepted 1st April 2026

DOI: 10.1039/d6su00101g

rsc.li/rscsus

Sustainability spotlight

Managing nitrogen cycle is one of the Grand Challenges of 21st century set forth by the National Academy of Engineers. As a nutrient for food production, nitrogen is critical to zero hunger (SDG2), but its reactivity and mobility in the environment results in detrimental impacts to human well being (SDG3) and the environment including clean water (SDG6). The work described here directly addresses these SDGs *via* atom-efficient method of synthesizing double salts from ammonium carbonate, recoverable from biomass digestate liquid, resulting in improved nitrogen management patterns of otherwise poor stability waste-derived nutrient containing materials.

Introduction

Nitrogen (N) is a cornerstone of agricultural productivity and global food security, yet its inefficient use remains one of the most persistent challenges across modern cropping systems.[1] Beyond agronomic inefficiencies, N management represents a broader resource-recovery challenge, as conventional N fertilizers such as urea and ammonium salts are produced through energy–intensive processes and dissolve rapidly following soil application.[2] This rapid dissolution generates

[a]Department of Chemical and Biomolecular Engineering, Lehigh University, 124 E. Morton St., Bethlehem, PA 18015, USA. E-mail: job314@lehigh.edu; Tel: +1-610-758-6836

[b]The Biodesign Institute Center for Environmental Health Engineering, Arizona State University, Tempe, AZ 85281, USA

[c]School of Sustainable Engineering and the Built Environment, Arizona State University, Tempe, AZ 85281, USA

[d]Agricultural Research Service, U.S. Department of Agriculture, Maricopa, AZ 85138, USA

† Both authors contributed equally.

transient pulses of plant-available N that are highly susceptible to loss through ammonia volatilization, nitrification-denitrification, and leaching.[3] These losses diminish fertilizer value while contributing to environmental degradation, including nitrate contamination of surface and groundwater and emissions of reactive nitrogen compounds. From a sustainable resource-management perspective, improving N use efficiency (NUE) is therefore essential for reducing nutrient waste, closing N loops, and aligning fertilizer design with circular-economy principles that couple materials innovation with agroecosystem performance.[4–7]

Anaerobic digestate represents one of the largest underutilized reservoirs of recoverable nutrients in modern agricultural and waste-management systems, particularly N.[8] During anaerobic digestion of livestock manures, food waste, and other organic residues, organically bound N is extensively mineralized, yielding digestate streams enriched in ammonium (NH_4^+) that can, in principle, substitute a substantial fraction of synthetic N fertilizers.[9–11] Despite this promise, digestate poses major challenges for agronomic reuse. Liquid digestate has low nutrient density, making it costly to transport and difficult to apply uniformly. In addition, its high ammoniacal N content makes it extremely prone to NH_3 volatilization during storage, handling, and land application, resulting in rapid N losses and secondary environmental impacts.[12,13] The recoverable N fraction in digestate is high and predictable, and recovery of N as ammonium carbonate has been demonstrated through distillation- or capacitive deionization-based processes that concentrate NH_4^+,[14] which can then be crystallized into a transportable solid phase, thereby extending the value chain of anaerobic digestion beyond biogas production.[15] Recovery of N as solid ammonium carbonate partially addresses these logistical constraints by converting dissolved NH_4^+ into a concentrated carrier; however, ammonium carbonate exhibits poor environmental chemistry when applied directly to soil. Its high solubility and instability lead to rapid dissociation and NH_3 volatilization, generating localized pH spikes that can be harmful to soil biota and further exacerbate N losses.[16] Consequently, while ammonium carbonate functions effectively as a solid NH_4^+ carrier recovered from digestate, it cannot be considered an agronomically safe or environmentally stable fertilizer in its native form and requires further formulation to moderate reactivity and protect soil biological integrity.[17,18] In addition, efficient plant uptake of recovered N is strongly mediated by the co-availability of other nutrients, particularly sulfur (S), which plays a critical role in N assimilation, protein synthesis, and enzymatic function.[19]

Mechanochemistry, which uses mechanical force to drive solid-state reactions, offers a sustainable alternative for producing solid engineered fertilizers without reliance on energy-intensive crystallization, while enabling tailored solubility and nutrient-release profiles. Through co-crystallization and the formation of double salts, mechanochemical synthesis can stabilize reactive nutrient ions into solid matrices that dissolve gradually, reducing loss pathways without requiring polymer coatings or high-temperature processing.[20] Recent work has demonstrated the mechanochemical synthesis of NH_4^+ double salts with magnesium (Mg) and zinc (Zn) carbonates, producing stable N–Mg and N–Zn fertilizers that showed reduced ammonia volatilization and improved N retention in soil.[21] Such processes can readily be scaled to tens of grams in laboratory planetary mills and, potentially, to industrial levels using continuous milling technologies.[22] Among the candidate materials that can serve to improve recovered ammonium carbonate properties, magnesium-ammonium-sulfate double salts[23] are of particular interest because they incorporate three agronomically important macro nutrients, N, Mg, and S, into a single solid phase.[24] Magnesium plays an essential role in photosynthetic processes and chlorophyll formation, while S is a key component of amino acids, cofactors, and enzymes required for N assimilation. Co-supplying these nutrients within a crystalline structure may therefore enhance both plant nutrition and NUE.[24–26] Despite their promising properties, the performance of mechanochemically synthesized magnesium ammonium sulfate (MgSA; $Mg(NH_4)_2(SO_4)_2 \cdot 6H_2O$) fertilizers under different soil conditions remains poorly understood.

This study evaluates a mechanochemically synthesized MgSA double salt as a potential sustainable N source and compares its behavior to urea and ammonium carbonate, $(NH_4)_2CO_3$, across three sandy loam soils with contrasting physicochemical properties. The novelty of this work lies in the mechanochemical synthesis of crystalline MgSA as a stabilized ammonium-bearing fertilizer phase and in demonstrating that its structural stabilization significantly reduces nitrogen loss compared with pure ammonium carbonate under humid and soil incubation conditions. Magnesium sulfate exists as a natural mineral, epsomite ($MgSO_4 \cdot 7H_2O$), as well as can also be recovered from brine.[27] We investigated fertilizer-induced differences in early lettuce development using biomass measurements, leaf chlorophyll content, image-based phenotyping, and soil N dynamics. Our objective was to determine whether MgSA provides more consistent N availability across soil environments and improves NUE relative to conventional fertilizers. By integrating soil chemistry, plant physiological responses, and fertilizer transformation dynamics, this work provides new insights into how mechanochemical co-crystallization can be leveraged to engineer next-generation fertilizers that enhance crop productivity while reducing environmental losses.

Materials and methods

Materials and synthesis

Chemicals and reagents. $MgSO_4 \cdot 7H_2O$ (Fisher Scientific), $MgSO_4$ (anhydrous, Eisen-Golden Laboratories), and ammonium carbonate $(NH_4)_2CO_3$ (Merck, Germany) were used as received. Ammonium carbonate material is commonly comprised of a complex mixture of related compounds, such as $(NH_4)_2CO_3$ and NH_4HCO_3, depending on the synthesis and storage conditions.[28] In this work, $(NH_4)_2CO_3$ (AC) was used as NH_4^+ feedstock.

Synthesis of $Mg(NH_4)_2(SO_4)_2 \cdot 6H_2O$. Laboratory scale 200 mg batches were synthesized using a Retsch MM300 mixer mill

equipped with a stainless steel 15 mL milling jar from Form-Tech Scientific (Canada) with a milling time of 10 min at 25 Hz using two 8 mm zirconia balls.[29] After the conversion was confirmed by powder X-ray diffraction (XRD), scaling up was performed using a Retsch PM100 planetary mill equipped with a 250 mL stainless steel jar, operated at 500 rpm for 30 min with 20 stainless steel balls and 20 g sample batches.

In addition to AC, two magnesium sulfate precursors, namely $MgSO_4 \cdot 7H_2O$ and anhydrous $MgSO_4$, were investigated. Several precursor-to-AC molar ratios were evaluated for each system. For $MgSO_4 \cdot 7H_2O$, the tested molar ratios were 1 : 1, 1.2 : 0.8, and 0.8 : 1. At the 1 : 1 molar ratio, the corresponding masses of $MgSO_4 \cdot 7H_2O$ and AC were 144.0 and 56.0 mg, respectively. For anhydrous $MgSO_4$, the molar ratio relative to AC was varied as 1 : 1, 1.5 : 1, and 2 : 1. At the 1 : 1 ratio, the masses of anhydrous $MgSO_4$ and AC were 111.0 and 89.0 mg, respectively. No additional water was introduced in the $MgSO_4 \cdot 7H_2O$ -based system, whereas the anhydrous $MgSO_4$ system required water to adjust the interaction, with 200 μL of water added to 200 mg of the reaction mixture in the small mill, and 20 mL added for the 20 g planetary mill experiments.

This approach avoids the need for energy-intensive solution crystallization while providing a rapid, reproducible, and environmentally benign synthesis method for fertilizer production. Mechanochemically synthesized samples were subsequently dried in a fume hood at room temperature for 24 hours.

The solution phase MgSA synthesis method involved dissolving ammonium sulfate, $(NH_4)_2SO_4$, and $MgSO_4 \cdot 7H_2O$ in bulk aqueous solution, followed by complete dissolution and overnight precipitation at room temperature.[23]

Physicochemical and functional characterization

Powder X-ray diffraction. The Cu K_α radiation with (λ = 1.5418 Å) (Empyrean X'pert PRO) was used to investigate the crystalline phases of the synthesized materials, while PANalytical software was utilized to collect the data. The scans were performed in the range of 5.0° to 50.0°, with a step size of 0.0131°, while the time per step is 15.3 s and the scan speed was 0.218838° s^{-1}. The applied voltage of the apparatus was 45 kV, while the current was 40 mA. The analysis was done with a mask of 4 mm, 1/16″ incident beam divergence slit, and 1/4″ incident beam anti-scatter slit.

Thermal analysis. Simultaneous thermogravimetric analysis and differential scanning calorimetry were performed from room temperature to 600 °C (PerkinElmer 7, USA). Measurements were conducted under a N_2 flow of 20 mL min^{-1} N_2 with a heating rate of 5 °C min^{-1}.

Elemental analysis. Surface elemental quantification was performed using XPS high-resolution O 1s, N 1s, S 2p and Mg 2p regions. XPS data was processed using the CasaXPS 2.3.27PR3.8 software suite.[30] Elemental quantification was carried out using Scofield relative sensitivity factors (RSF).[31] The inelastically scattered background was subtracted using Shirley's background method.[32]

Particle morphology and bulk spectroscopic analysis of MgSA was performed using field emission scanning electron microscopy (FESEM, Hitachi S-4300SE/N Electron microscope) using an accelerating voltage of 5 kV in combination with energy dispersive spectrometry (EDS, 30 mm^2 EDAX Octane Elect Plus) using an accelerating voltage of 15 kV. Bulk Mg, N and S analysis was performed using standard Association of Official Analytical Collaboration (AOAC) 2017.02 ICP, AOAC 993.13 and AOAC 2017.02 methods.

Laboratory mechanical properties. Approximately 300 mg of MgSA or $(NH_4)_2CO_3$ powder were compressed into pellets by uniaxial pressing at 3000 psi for 1 min. The resulting pellets exhibited uniform geometry, with dimensions in the range of 5–7 mm. To evaluate the effect of relative humidity on fracture strength, replicate pellets were stored in a desiccator maintained at 70% relative humidity (RH).

The maximum compressive stress of each pellet was determined by a uniaxial compression test using Mxmoonfree mechanical testing system (HP-500N). Measurements were conducted daily to monitor temporal changes in mechanical strength over time. Each experiment was repeated using multiple pellets, and the results are reported as the mean value with the corresponding standard deviation.

Laboratory nitrogen release kinetics measurements

The volatilized nitrogen loss from MgSA pellets was evaluated in comparison with pure AC pellets using a soil surface incubation experiment conducted at 90% relative humidity (RH), following the previous work approach.[33] The experimental setup consisted of four independent soil columns, each containing 130 g of fresh soil. Moist air was supplied to each column at a controlled flow rate of approximately 1.5 L min^{-1} using an air pump. The humidified air was directed over the soil surface, onto which MgSA and AC pellets were placed. The masses of MgSA and ammonium carbonate (AC) were adjusted to provide an equivalent N loading of 0.184 g N per 130 g of soil (1.42 mg N $g\ soil^{-1}$). The outlet air from each column was subsequently passed through a trapping solution containing 0.2 N sulfuric acid to capture volatilized NH_3. The collected NH_4^+ was quantified using standard alkaline titration. Experiments with MgSA were conducted in triplicate using three parallel columns, while AC was analyzed simultaneously in the fourth column as a control.

An examination of the N release kinetics from MgSA was conducted using the Richards model.[34,35] The Richards function uses four functional parameters. These parameters enable a comprehensive and detailed depiction of the cumulative frequency distribution (cumulative nitrogen release).[36] In this study, we employed a unified methodology based on the Richards model.[37] This method facilitates the comparison of different fertilizers, enabling the assessment of varied N-release curves without requiring any additional adjustments or conversions.[33] The unified Richards model is defined in eqn (1)

$$W(t) = A\left(1 + \left(\left(\frac{W_o}{A}\right)^{1-d} - 1\right)\cdot\exp\left(-\frac{k\cdot t}{d^{\frac{d}{1-d}}}\right)\right)^{\frac{1}{1-d}} \quad (1)$$

where $W(t)$ represents the amount of N (%) released at a time (t, days), A denotes the upper asymptote (the maximum or end point of net N released, %), W_o is the initial value at the beginning of the observation period (%), k refers to the slope at the inflection point (the point where the rate of N release is highest), and d is the parameter that determines the shape of the curve. The fitting analysis was conducted using, the curve_fit() function in Python library SciPy (version 1.13.0) optimize module as described in previous work.[33]

Agricultural pot experiments

Agricultural site and soils used. The study was conducted in a growth chamber at the US Arid Land Agricultural Research Center (ALARC), USDA. Surface soil samples (0–20 cm) were collected from Arizona (AZ) and North Carolina State (NC). Three Sandy Loam soils (Table 1) were collected at ALARC, Maricopa, AZ (soil A), Horticultural Crops Research Station, Clinton, NC (soil B) and Oxford Tobacco Research Station, Oxford, NC (soil C). Following collection, soils were transferred to a greenhouse at ALARC, placed in bins, and covered with plastic for solarization. After 2.5 weeks, the bins were uncovered, and the soils were air-dried. The dried soils were ground and sieved to a maximum particle size of 2 mm.

Levels of N were adjusted based on the results of the soil analysis and following the Guidelines for Head Lettuce Production in Arizona (ACIS).[38] Phosphorus (P) and potassium (K) levels varied from high to medium among the soil samples; no P or K was added.

A starter N application corresponding to 20% of the total recommended rate was applied prior sowing. To achieve the target concentration of 0.05 g N Kg^{-1} soil, 0.19 g of urea (UR – 46% N), 0.39 g of Ammonium carbonate (AC – 23% N) and 1.2 g of $Mg(NH_4)_2(SO_4)_2 \cdot 6H_2O$ (MgSA – 7.3% N) were thoroughly mixed with 1.8 kg of soil. All fertilizer materials were previously analyzed for N concentration and applied in powder form. A no-N control was also included.

For the assays, 150 g of soil air-dried and processed was placed in pots (6 × 6 × 6 cm). Three romaine lettuce seeds were sown per pot. The experiment followed a completely randomized design with eight replicates. Pelleted 'Sparx' Romaine lettuce seeds were purchased from Johnny Seeds, product ID: 3156JP. Ten days after emergence, seedlings were thinned, leaving the largest one per pot. Throughout cultivation, the soil moisture was maintained at approximately 90% of field capacity with daily irrigation with deionized water to replace evapotranspiration losses, determined gravimetrically. Plants were grown in a CONVIRON growth chamber (CMP6060) under controlled environmental conditions. Air temperature was maintained at 17.2 °C during the dark period (00 : 00–06 : 30) and 28 °C during the light period (06 : 31–23 : 59). Photosynthetically active radiation (PAR) followed a stepped diurnal profile: 0 μmol m^{-2} s^{-1} from 18 : 31–06 : 00; 200 μmol m^{-2} s^{-1} from 06 : 01–06 : 30; 600 μmol m^{-2} s^{-1} from 06 : 31–16 : 00; 500 μmol m^{-2} s^{-1} from 16 : 01–17 : 30; and 200 μmol m^{-2} s^{-1} from 17 : 31–18 : 30. Relative humidity was maintained at 60%.

Table 1 Physical and chemical properties of the soils used in the study[a]

Soil	Sand g kg^{-1}	Clay g kg^{-1}	Silt g kg^{-1}	pH	Lime 0.1 ton $acre^{-1}$	Phosphorous mg kg^{-1}
A	6.53	1.23	2.23	8.5	NA	360.0
B	6.9	1.67	1.43	5.5	1.6	254.6
C	8.5	0.3	1.2	5.9	1.2	116.3

Soil	OM g kg^{-1}	Free lime	Nitrate mg kg^{-1}	Total nitrogen mg kg^{-1}	Sodium mg kg^{-1}	Potassium mg kg^{-1}
A	0.02	Low	24	290	160	24.5
B	0.16	None	10	590	7.9	32.1
C	0.07	None	9.3	450	19	41.8

[a] OM-Organic matter.

Soil analysis. Prior to the start of the experiment, each soil was analyzed and following plant harvest, the soil in each pot was thoroughly homogenized and a representative sample withdrawn, oven dried at 65 °C and analyzed. Inorganic N and exchangeable acidity were extracted using KCl, and N levels were quantified as nitrates. For all three soils, pH (H_2O) and electrical conductivity (EC) were determined in a soil: water suspension (1 : 1, m/v). Organic matter was determined by the loss-on-ignition method and total N in soil was determined using the Kjeldahl method.[39]

For soil A, potassium (K), calcium (Ca), Mg, and sodium (Na) residing on the soil colloid exchange sites were extracted by displacement with ammonium acetate solution buffered to pH 7.0. Cation concentrations are determined using atomic emission (AES), absorption spectrometry (AAS), or ICP-AES instrumentation. Copper (Cu), manganese (Mn), boron (B) and zinc (Zn) were extracted using the DTPA (diethylenetriaminepentaacetic acid) micronutrient extraction method, developed by Lindsay and Norvell[40] for neutral and calcareous soils. Nitrate (NO_3) and exchangeable acidity were extracted using KCl. Phosphate-P and PO_4-P were quantified according to Olsen.[41] Phosphate from the soil was extracted by a 0.5 N sodium bicarbonate solution adjusted to pH 8.5. Sulfate-S, SO_4-S, was determined according to Schulte and Eik[42] with the following exception: (1) elimination of activated carbon and (2) determination of S by ICP-AES.

For soil B and C, the nutrients K, Ca, Na, Cu, Mn, Zn, P and NO_3 were determined using Mehlich III.[43]

Image analysis. A 16 MP Olympus TG-4 camera (Olympus Corporation, Tokyo, Japan) was employed to photograph plants inside a lightbox. The camera was held in nadir orientation approximately 30 cm distant. Images were recorded in normal quality JPEG format (approximately 5.4 MB), with a resolution of 4608 × 2592 pixels (16 : 9 aspect ratio). Photographic exposure settings were set by an ISO of 200, aperture f/8, and automatic shutter speed ranging from 1/40 to 1/200 seconds. The camera operated with single auto focus and natural mode automatic white balance. A total of 96 images were captured.

Image-derived color variables. Image processing was conducted using Python 3.12 software (Python Software

Foundation, Beaverton, OR, USA) based on OpenCV 4.10.0[44] and Scikit-image 0.23.2[45] packages using a customized approach.[46] Images were processed on a Dell Precision 7680 laptop with an i9-13950 H × 2.2 GHz CPU and 64 GB of RAM (Dell Technologies Inc., Round Rock, TX, USA) running Microsoft Windows 11 Enterprise 64 bit OS (Microsoft Corporation, Redmond, WA, USA). It took approximately 4 minutes to process each image. MS Excel Version 2510 (Microsoft Corporation, Redmond, WA, USA) was used to manage tables of results.

Pixels containing green living plant material were segmented from the images using color filter thresholding in the HSV (Hue saturation salue) color space. Pixels representing vegetation were selected if the Hue angle was between 30 and 60 (on a scale of 1 to 180), Saturation was between 75 and 255 (on a scale of 0 to 255) and brightness Value was between 1 and 254 (on a scale of 0 to 255). The green filter parameters were determined iteratively by evaluating pixel selections for multiple sample images. This approach allowed identification of an optimal filter parameter set that best accounted for the visible living green plant material and follows the method of Karcher.[47]

The fraction of green area was based on the ratio of green pixel count to the total pixel count. To assess color qualities, image calculations were performed only on the fraction of green living plant material segmented from sample images. The Aggregate Chromaticity Index (ACI) was calculated as the sum of the u^* and v^* chromaticity components ($ACI = u^* + v^*$) derived from the perceptually uniform CIELUV color space. These parameters are independent of illumination and represent chromatic variation along red-green and yellow-blue axes, respectively. Therefore, ACI provides an integrated measure of color variation associated with red-green dominance. This relationship has been identified as a strong and consistent indicator of plant color response in previous analyses.[21]

Chlorophyll measurements. Leaf disks (0.6 cm) were collected and immediately placed on ice, then stored in −20 °C for further analysis. Total chlorophyll content (chlorophyll a + chlorophyll b) in lettuce leaves was measured according to the method described by Hiscox and Israelstam[48] and calculated with an adjusted formula by Wellburn.[49] Briefly, pre-weighed frozen leaf discs were incubated at 65 °C in dimethyl sulfoxide (DMSO) until complete tissue bleaching was achieved. Absorbance of the resulting solution was measured at 649 and 665 nm to quantify chlorophyll contents.

Statistical analysis. All statistical analyses were performed in R (version 4.5.2), with additional data handling in Microsoft Excel. For each response variable (biomass, chlorophyll content, image-derived color indices, soil nitrate, and total soil nitrogen), soil type and N treatment were modeled as fixed categorical factors in a two-way analysis of variance (ANOVA). Prior to interpreting results, ANOVA assumptions were evaluated through inspection of model residuals, including quantile–quantile plots for normality, residual-versus-fitted plots for homoscedasticity, and leverage diagnostics to identify influential observations. No substantial deviations were detected; therefore, all variables were analyzed without transformation.

When the ANOVA indicated significant main or interactive effects ($P < 0.05$), post-hoc comparisons were conducted using Tukey's Honestly Significant Difference (HSD) test as implemented in the agricolae package.[50] To facilitate the interpretation of factorial responses, grouping letters were generated separately for each factor. These groupings were obtained by subsetting the dataset by factor level and extracting agricolae HSD group outputs.

Results and discussion

MgSA synthesis from hydrated magnesium sulfate, $MgSO_4 \cdot 7H_2O$, and AC

The first experiment set focused on using a common mineral, epsomite ($MgSO_4 \cdot 7H_2O$), as an Mg- and S-precursor for the synthesis of the MgSA double salt. This precursor is heptahydrate and hence can balance the overall chemical reaction by providing all six water molecules that are included in the MgSA crystal. Neat mechanochemical experiments were performed after mixing dry $MgSO_4 \cdot 7H_2O$ and AC, and the extent of the reactant conversion was monitored by *ex-situ* pXRD analysis. The mechanochemical conditions using the shaker mill are optimized for double salt synthesis, so no significant temperature increase is observed. $(NH_4)_2CO_3$ crystal is expected to undergo facile ion release during milling with NH_4^+ ion incorporated into the double salt structure, while carbonate decomposes to CO_2. Similar double salt crystalline structures, such as $Mg(NH_4)_2(CO_3)_2 \cdot 4H_2O$, were shown to exist in excess of $MgCO_3$ during the synthesis with (101), (111), (200) and (220) reflections between $2\theta = 14$ and 28°,[51] but the primary reflections of MgSA are very dominant in Fig. 1 at all $MgSO_4 \cdot 7H_2O$ and AC ratios. The conversion was complete with no reactant peaks observed in the product spectra and the ratio of the reactants did not play a role within the molar $MgSO_4 \cdot 7H_2O$: AC of 0.8 : 1.2 to 1.2 : 0.8. While amorphization of ionic compounds, such as calcium phosphate, has been reported under extreme mechanical stress (~10 GPa) in the literature,[52]

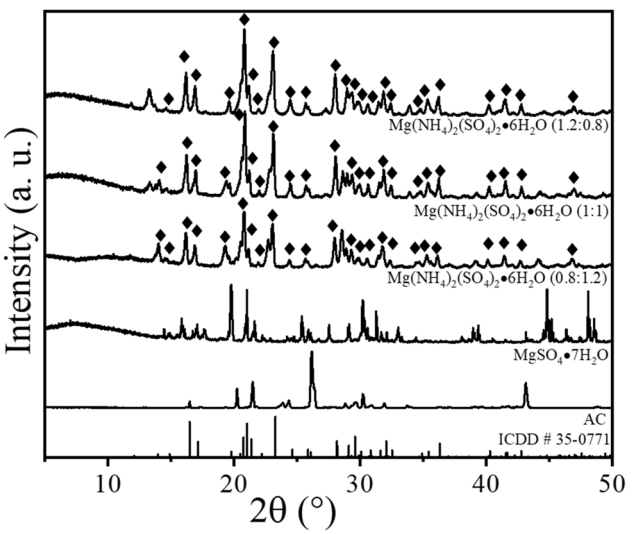

Fig. 1 Experimental pXRD patterns of reactants ($MgSO_4 \cdot 7H_2O$ and AC) and the products obtained from small-scale mechanochemical synthesis of MgSA using different molar $MgSO_4 \cdot 7H_2O$ and AC ratios. The theoretical bar pattern of MgSA is also provided. (◆:MgSA).

and may similarly occur here, potentially obscuring the crystalline features in pXRD, the results nonetheless indicate that crystalline MgSA forms as a primary product.

Synthesis from anhydrous $MgSO_4$ precursor and AC

Anhydrous $MgSO_4$ is hygroscopic and can be obtained from $MgSO_4 \cdot 7H_2O$. As shown in Fig. 2, MgSA was synthesized starting from the anhydrous $MgSO_4$ phase. A controlled amount of water (40 μL per 200 mg of precursors) was added to facilitate the formation of MgSA containing six water molecules. However, the resulting product exhibited relatively poor crystallinity compared with MgSA synthesized directly from $MgSO_4 \cdot 7H_2O$. In contrast, scale-up synthesis using a larger batch (20 g) of $MgSO_4$ and AC with a substantially higher water content (20 mL) resulted in the formation of highly crystalline MgSA. These observations indicate that water content plays a critical role in promoting phase-pure crystallization of MgSA.

Thermal properties of MgSA

Ammonium carbonate exhibits relatively low thermal stability, undergoing a complete decomposition at a temperature of 130 °C, as shown in Fig. 3a. Furthermore, at a temperature of 100 °C, it has lost about 50% of its initial mass. It exhibits two endothermal peaks at 88 and 125 °C in Fig. 3b associated with the quick transformation into ammonium bicarbonate, followed by its complete decomposition. Anhydrous $MgSO_4$, on the other hand, is very stable up to 600 °C and loses virtually no mass, as shown in Fig. 3a.

The total molar mass of MgSA is 360.6 g mol^{-1}, with each coordinated water molecule contributing approximately 5.0 wt% to the total mass. The TGA reveals three distinct mass-loss regions upon heating. The first mass-loss event occurs at approximately 152 °C, where the mechanochemical MgSA loses about 24 wt% of its initial mass. This value closely corresponds to the release of five water molecules. The DSC curve shows an endothermic peak around 117.5 °C, which confirms the dehydration reaction. The exothermic peak at approximately 225 °C, observed for both mechanochemical MgSA and solution-derived MgSA, is attributed to the crystallization of a dehydrated intermediate phase formed after water removal. The second mass-loss step is observed around 320 °C and is associated with an additional mass reduction of approximately 10 wt%. This loss is consistent with the simultaneous removal of the remaining strongly bound water molecule together with partial deammoniation, most plausibly through the evolution of NH_3. This stage, therefore, marks the transition from dehydration to ammonium decomposition.

At higher temperatures, a third mass-loss region leads to the formation of a plateau starting at approximately 450 °C, with a further mass loss of about 16 wt%. Beyond this temperature, no significant mass change is detected under a nitrogen atmosphere, indicating the formation of a thermally stable residue. Considering that anhydrous $MgSO_4$ accounts for approximately 33 wt% of the original MgSA mass, the observed plateau supports the conclusion that the final solid residue is predominantly $MgSO_4$. The slightly higher residual mass compared to the theoretical value suggests that the mechanochemically synthesized MgSA may retain a sulfate-rich, non-stoichiometric intermediate or partially condensed sulfate species, rather than transforming into perfectly stoichiometric $MgSO_4$ at this temperature. Overall, mechanochemically synthesized MgSA exhibits 50.5% mass loss while MgSA obtained *via* precipitation exhibit 62.5% mass loss.

The first endothermal peak in Fig. 3b in mechanochemically synthesized MgSA coincided with that obtained *via* the precipitation method, suggesting that about 24% mass loss occurred due to the dehydration. No lower temperature endothermal processes were observed, suggesting conversion of ammonium carbonate to more stable MgSA. A single exothermal peak at 225 °C in Fig. 3b was common to both mechanochemically synthesized and precipitated MgSA due to its transformation to efremovite $Mg_2(NH_4)_2(SO_4)_3$.[23] Endothermal peaks above 300 °C have previously been suggested to occur due to the dehydrated NH_4HSO_4 decomposition.[53]

In this regard, Y. Ma *et al.* synthesized several double salts based on MgSA and investigated their thermal stability. The results showed that MgSA started decomposition by Lossing the water bonded molecules, while the maximum weight loss was about 70% at 600 °C, compared to 50.5% in case of our mechanochemically derived MgSA.[53]

As shown in Fig. 3c, Raman spectra of both mechanochemically synthesized and precipitated MgSA exhibited identical SO_4^{2-} peaks at 980 cm^{-1}, but different spectral envelopes in the 2750–3750 cm^{-1} region. The water content of the precipitation derived MgSA seems to be higher than the mechanochemical MgSA, which is confirmed from TGA and matches well with the H_2O region in Raman spectra. Thermal analysis suggested that mechanochemically synthesized MgSA exhibits properties of conventional precipitated material.

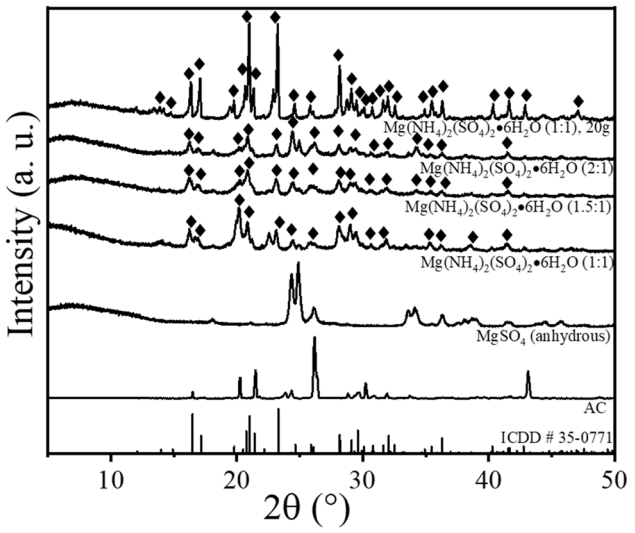

Fig. 2 Experimental pXRD patterns of reactants (anhydrous $MgSO_4$ and AC) and the products obtained from small-scale mechanochemical synthesis of MgSA using different molar anhydrous $MgSO_4$ and AC molar ratios as well as planetary mill synthesized 20 gram batch using $MgSO_4$: AC = 1 : 1. The theoretical bar pattern of MgSA is also provided. (◆:MgSA).

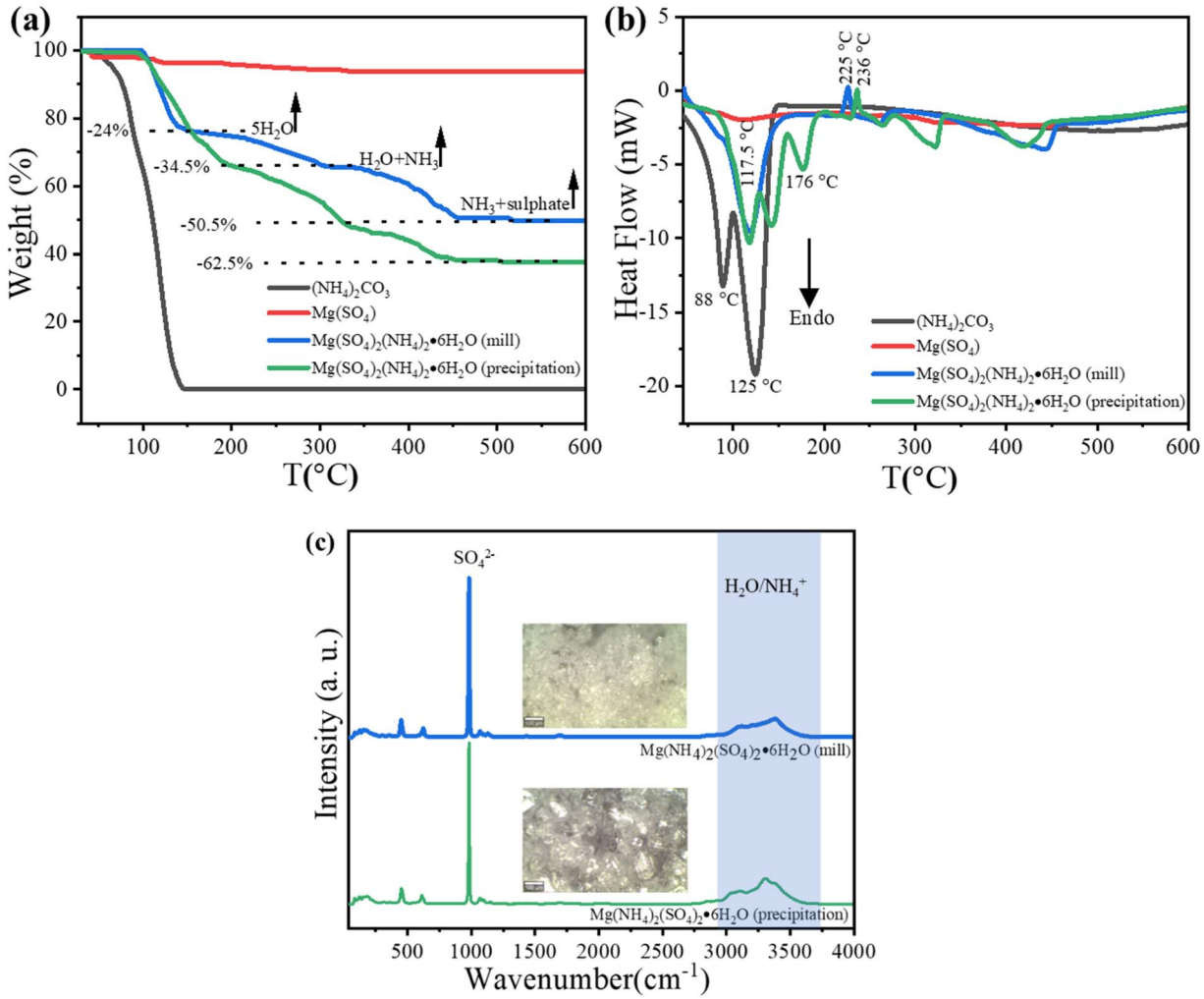

Fig. 3 (a) Thermogravimetric analysis (TGA), (b) differential scanning calorimetry (DSC) and (c) Raman spectroscopy analysis of MgSA and the corresponding reactants. MgSA synthesized using the precipitation method from aqueous solution is also shown.[53]

Bulk chemical composition of MgSA

Chemical composition analysis of MgSA yielded 7.3 weight % N, close to the stoichiometric value of 7.8% as shown in Fig. 4. Spatially resolved EDS analysis suggested a uniform element distribution within particulate aggregates of sub-10 μm in size.

Surface chemical composition of MgSA

XPS analysis was performed on the mechanochemically synthesized MgSA to elucidate its chemical composition. Mechanochemical reactions involve exposing fresh, high-energy surfaces, which accelerate the reaction while fresh surfaces are exposed.[54] The survey spectrum of MgSA in Fig. 5 shows Mg and O-rich surface with S and N comprising about 10% and 7 atomic %. This was in qualitative agreement with EDS results shown in Fig. 4. O 1s peak at ~532.0 eV was assigned to the SO_4^{2-} group in $MgSO_4$ (ref. 55) concomitant with the S 2p peak at ~169 eV and Mg 2p peak at 50.5 eV. C 1s exhibited two peaks due to the C–C bonds (adventitious carbon) at ~285 eV and CO_3^{2-} at 290.0 eV,[56] suggesting residual carbonate ions on the surface. The peak in N 1s at 401.5 eV can be assigned to NH_4^+ groups present on the surface.[57] XPS analysis confirmed the presence of nutrient-related elements on the MgSA surface and provided insight into their surface chemical states.

Laboratory nitrogen loss properties *via* NH_3 measurements

Fig. 6a shows NH_3 release patterns measured for ammonium carbonate and mechanochemically synthesized MgSA in the presence of 90% RH over a 16 days period. The amount of N added was 0.184 g/130 g of soil (1.42 mg N per g soil). It can be observed that ammonium carbonate released ~50% of N as NH_3 within 2 days, consistent with the observations of its low environmental stability.[16] The maximum amount of NH_3 released slowed down and was measured at 70% after 16 days. MgSA resulted in much slower NH_3 release kinetics, especially in the early stages, with about 50% of N lost as NH_3 after 16 days.

Experimental laboratory N loss experiments shown in Fig. 6 were fitted with the Richards model.[58,59] Parameter *A* denotes the upper asymptote (the maximum or end point of net N released, %), *k* refers to the slope at the inflection point (the

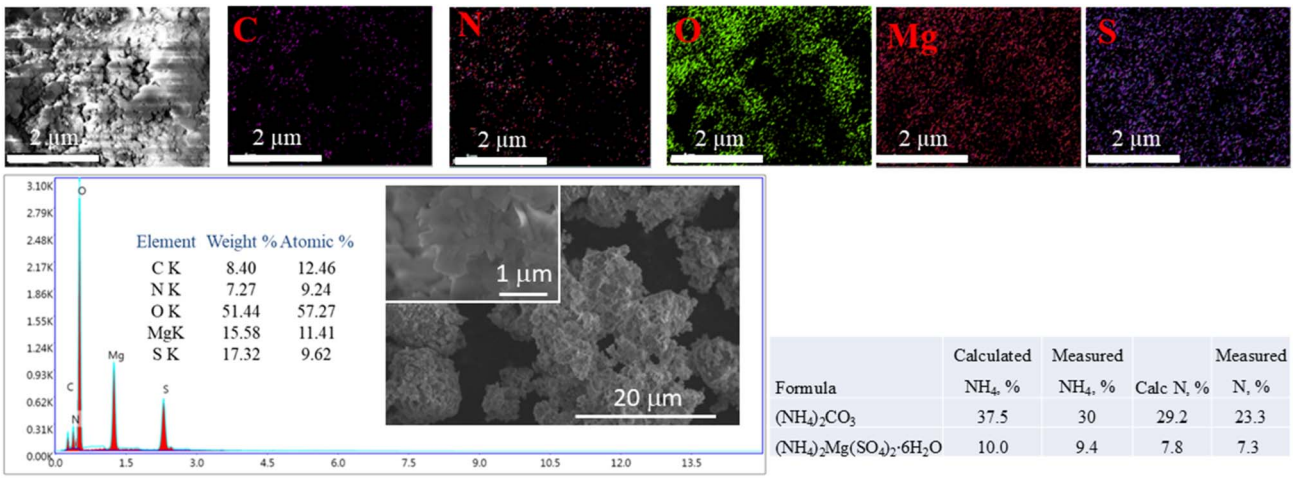

Formula	Calculated NH_4, %	Measured NH_4, %	Calc N, %	Measured N, %
$(NH_4)_2CO_3$	37.5	30	29.2	23.3
$(NH_4)_2Mg(SO_4)_2{\cdot}6H_2O$	10.0	9.4	7.8	7.3

Fig. 4 Spatially resolved SEM images, energy dispersive and bulk chemical analysis of mechanochemically synthesized MgSA.

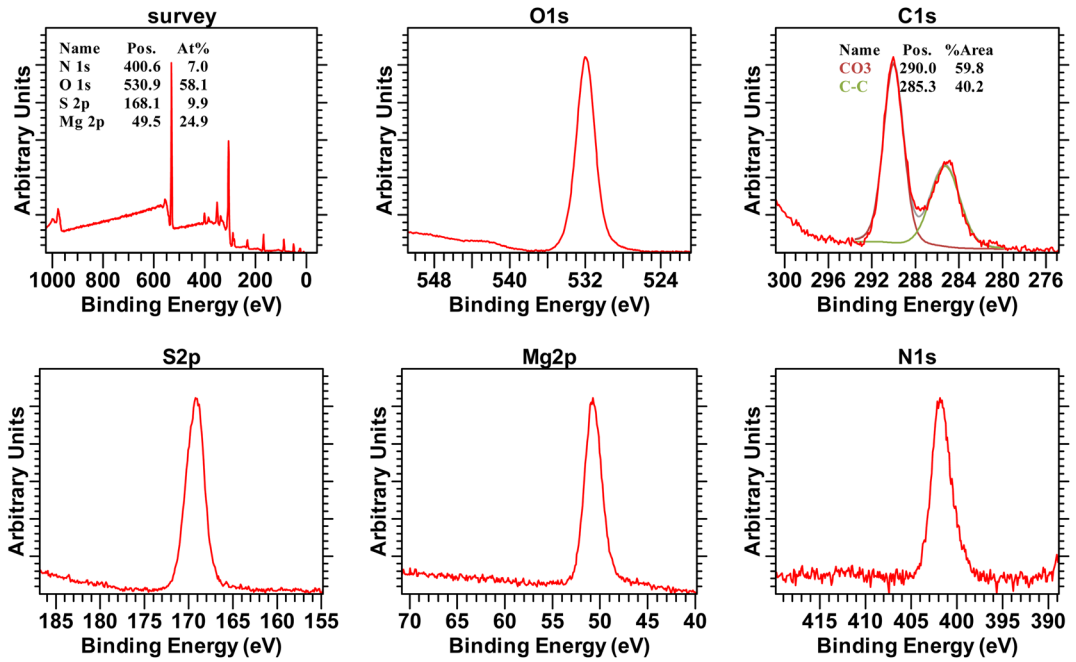

Fig. 5 XPS surface analysis of mechanochemically synthesized MgSA.

point where the rate of N release is highest) and d is the parameter that determines the shape of the curve. It can be seen that A was 64.8% in ammonium carbonate and 57.5% in MgSA after 16 days, but the kinetics of the release were significantly different. Parameter k was 0.1 for MgSA, lower than 0.6 in ammonium carbonate, suggesting kinetically limited N release properties.

Compressive strength properties of MgSA pellets

Compressive strength was tested of the pelletized ammonium carbonate and MgSA as synthesized and after 2 days under constant 70% RH, as shown in Fig. 7. Fracture strength was measured and ammonium carbonate pellets exhibited very low strength of ~2 MPa. As synthesized pelletized MgSA exhibited fracture strength of ~18 MPa, which gradually decreased to 15 MPa with storage at 70% RH. Ammonium carbonate granules disintegrated after day 1 storage.

Nitrogen dynamics in soil *via* field measurements

Soil chemical environments play a decisive role in determining N fate and fertilizer efficiency.[3,60] High-pH, sodium-rich soils promote ammonia volatilization and can impose salinity stress,[61–63] both of which suppress plant growth and reduce effective N uptake.[64–66] Conversely, acidic soils can limit nutrient availability and root metabolic activity if not properly limed.[67,68] These contrasts make lettuce, a fast-growing, shallow-rooted

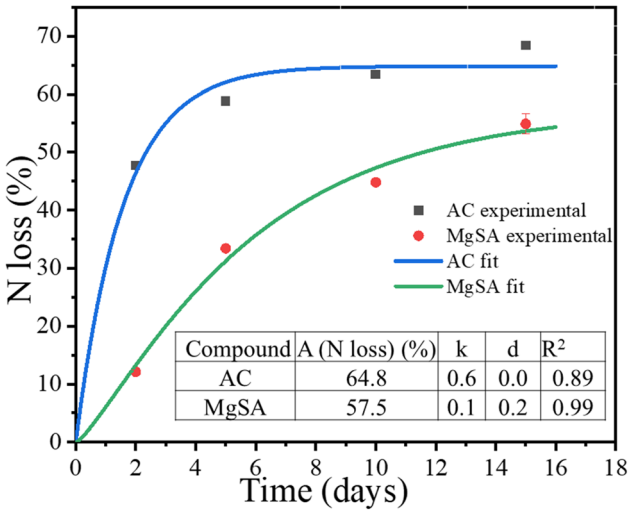

Fig. 6 Mechanochemically synthesized MgSA nitrogen loss over time measured as NH_3, while the continuous lines represent the nitrogen volatilization losses of MgSA fitted with the unified Richards model.[58,59]

crop highly responsive to early-season N availability, an interesting system for testing the performance of engineered N fertilizers across divergent soil conditions.[69,70]

The three soils used in this study exhibited contrasting physicochemical characteristics that strongly influenced fertilizer behavior and plant responses (Table 1 and Fig. 8a, b). Soil A was highly alkaline (pH 8.5), extremely low in organic matter, and contained detectable free lime and elevated sodium, a combination known to promote ammonia volatilization and depress ammonium retention.[61,71–74] The elevated sodium levels in Soil A likely contributed to salinity-induced stress, which can impair water uptake, reduce leaf expansion, and suppress early vegetative growth in lettuce, which explains the reduced growth as compared to soil C.[75,76]

In contrast, soils B and C were moderately acidic (pH 5.5–5.9) and contained higher organic matter and lower sodium concentrations, conditions generally more favorable for ammonium stabilization and microbial N transformations.[77–79] However, despite its moderate acidity, soil B also exhibited reduced growth relative to soil C, likely reflecting constraints associated with lower pH and insufficient liming requirement, which can reduce root metabolic activity and limit nutrient availability during early seedling establishment.[67,80,81] Baseline nitrate and total soil N also varied among soils, indicating inherent differences in mineral N availability prior to fertilizer addition (Table 1).

Lettuce shoot biomass at 23 days after sowing responded strongly to N source, and the magnitude of these differences varied across soils (Fig. 8 a and b). In all soils, the control without added N produced the smallest plants, confirming N limitation during early vegetative growth. Urea (UR), MgSA ($Mg(NH_4)_2(SO_4)_2 \cdot 6H_2O$) and ammonium carbonate (AC) increased biomass but showed marked soil-dependent behavior (Fig. 8a and b).

Across all three soils, mechanochemically synthesized double salt MgSA generated consistently high biomass, often matching or exceeding that of urea and AC despite providing substantially less total N per unit mass. This cross-soil consistency suggests that the crystalline Mg–NH_4–SO_4 framework moderated N release in a way that buffered plants from soil-driven N losses. The stabilized structure of the hydrated double salt likely slowed dissolution and limited rapid ammonium volatilization in alkaline Soil A, while simultaneously ensuring a steady supply of available N in the more acidic soils. The co-provision of Mg^{2+} may have further supported early growth by contributing to chlorophyll synthesis and photosynthetic function, especially in soils with low inherent nutrient reserves.[82,83]

Canopy color metrics supported these biomass responses. Chlorophyll content and image-derived Aggregate Chromaticity Index (ACI) demonstrated that overall MgSA-treated plants maintained greener canopies than those receiving AC and exhibited color properties comparable to urea across soils (Fig. 9b).

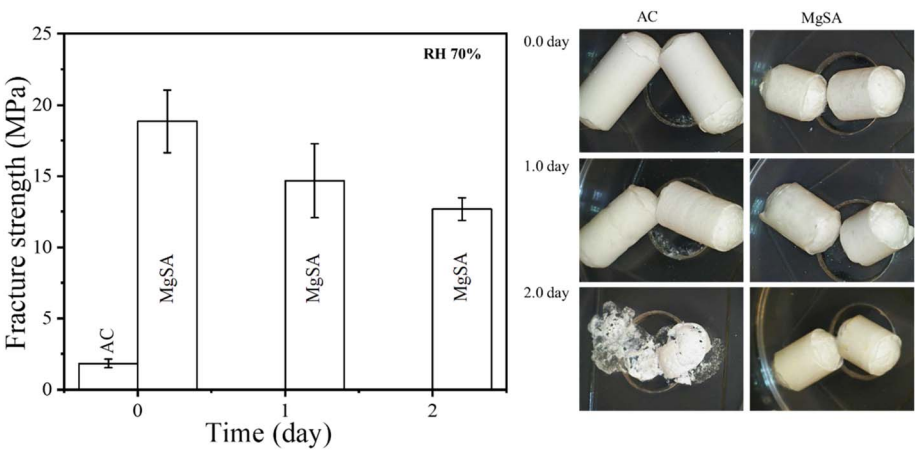

Fig. 7 Compressive strength measurements of ammonium carbonate and MgSA pellets as synthesized and after storage in the presence of 70% RH. Error bars represent triplicate independent measurements.

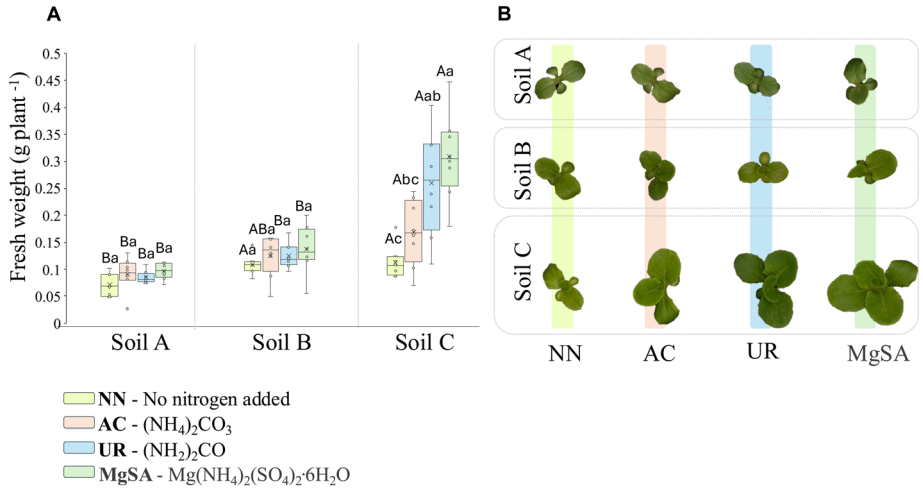

Fig. 8 Plant growth response to engineered fertilizer treatments under controlled conditions. Lettuce shoot biomass (A) at 23 days after sowing following application of urea (UR), ammonium carbonate (AC), and mechanochemically synthesized magnesium ammonium sulfate double salt MgSA ($Mg(NH_4)_2(SO_4)_2 \cdot 6H_2O$). Values represent the average of eight replicates ± standard error. Different letters indicate significant differences according to Tukey's HSD test ($p < 0.05$): lowercase letters denote differences among treatments within the same soil, and capital letters. (B) Representative images of lettuce plants grown in each soil under the different fertilizer treatments at 23 days after sowing.

These findings underscore that MgSA delivered sufficient N to sustain high physiological activity during early growth. The enhanced greenness also reflects the bioavailability of Mg^{2+}, an essential component of chlorophyll molecules, indicating that this mechanochemical fertilizer provided multiple growth-limiting nutrients in a synchronized manner.[83] Additionally, sulfur (S) plays a central role in enhancing N uptake and utilization by serving as an essential constituent of amino acids, cofactors, and enzymes involved in plant N assimilation.[84,85]

Adequate S supply supports the synthesis and activity of key metabolic enzymes such as nitrate reductase and glutamine synthetase, thereby improving the conversion of inorganic N into organic forms. Sulfur also contributes to soil chemical processes that influence nutrient retention and availability, and in legumes, it supports the formation and function of nitrogen-fixing nodules by promoting nodule protein synthesis and symbiotic enzyme activity. Through these biochemical and physiological pathways, S availability increases NUE, enabling plants to more effectively assimilate absorbed N and translate it into biomass.[84,86,87] The imaging data, therefore, corroborate the observed biomass trends and further illustrate the agronomic value of controlled ammonium release.

Soil nitrate and total N concentrations 23 days after sowing revealed additional insights into fertilizer transformation dynamics (Fig. 10a and b). Urea produced higher nitrate levels in most soils, consistent with its rapid dissolution and

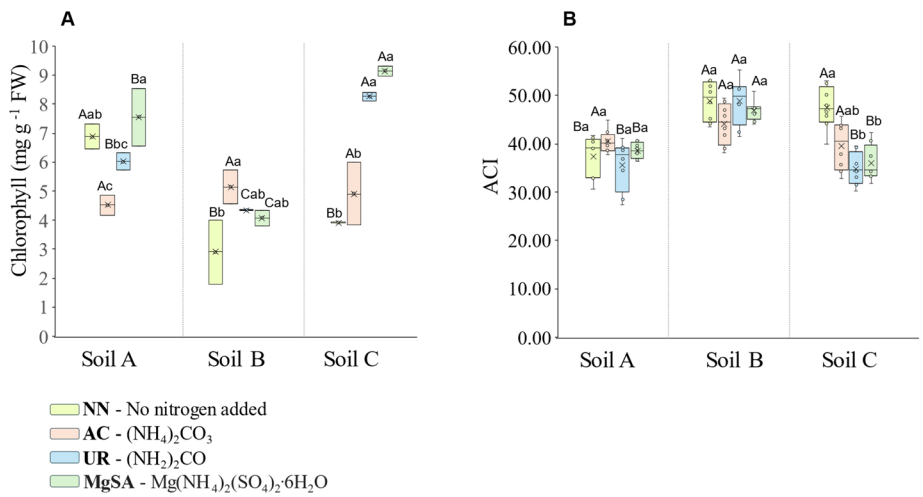

Fig. 9 Chlorophyll content (A) and image-derived color indices (B), aggregate chromaticity index (ACI), for different nitrogen sources, urea (UR), ammonium carbonate (AC), and mechanochemically synthesized magnesium ammonium sulfate double salt MgSA MgSA ($Mg(NH_4)_2(SO_4)_2 \cdot 6H_2O$). Values represent the average of three and eight replicates, respectively. Different letters indicate significant differences according to Tukey's HSD test ($p < 0.05$): lowercase letters denote differences among treatments within the same soil, and capital letters denote differences among soils within the same treatment.

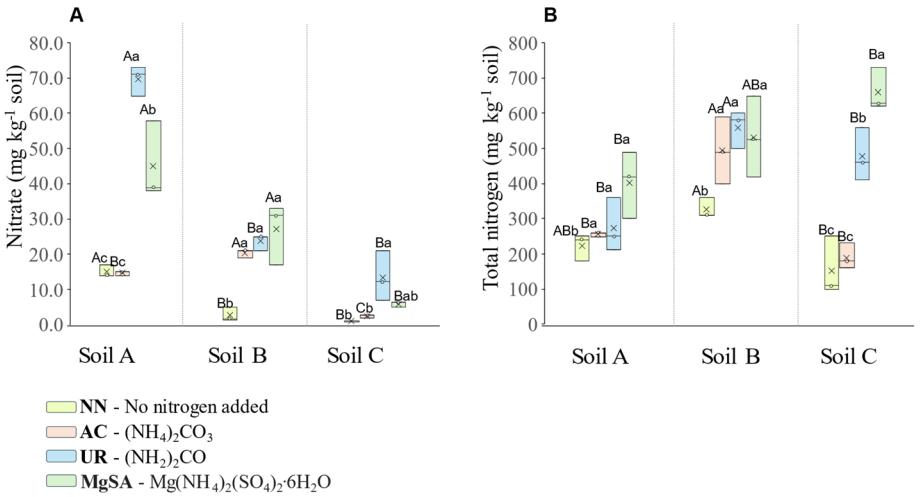

Fig. 10 Nitrate (A) and total nitrogen (B) in soil 23 days after sowing for different nitrogen sources urea (UR), ammonium carbonate (AC), and mechanochemically synthesized magnesium ammonium sulfate double salt MgSA MgSA ($Mg(NH_4)_2(SO_4)_2 \cdot 6H_2O$). Values represent the average of three replicates. Different letters indicate significant differences according to Tukey's HSD test ($p < 0.05$), lowercase letters denote differences among treatments within the same soil, and capital letters denote differences among soils within the same treatment.

immediate conversion to ammonium, followed by swift nitrification. While this rapid release can supply abundant early N, it also generates a large pool of mineral N susceptible to leaching and denitrification, especially in coarse-textured soils under frequent irrigation. MgSA, in contrast, resulted in lower soil nitrate accumulation in most soils as compared to urea. This pattern is consistent with slower ammonium release from the double-salt matrix and reduced substrate availability for nitrifying microbes. The combination of high plant biomass and low soil nitrate suggests that most of the N liberated from MgSA was taken up by plants rather than accumulating in the soil, thereby indicating improved synchronization between N release and crop demand. MgSA resulted in the highest total soil N concentration in Soil C, the only soil in which plants exhibited vigorous growth, 23 days after sowing, outperforming all other N sources. Although the differences were not statistically significant in soils A and B, the same trend was observed, with MgSA maintaining slightly higher residual total N relative to urea and ammonium carbonate (Fig. 10b).

The behavior of MgSA across soils with pH spanning from moderately acidic to strongly alkaline highlights an important advantage of mechanochemical co-crystallization. Whereas the performance of UR and AC appeared strongly influenced by soil conditions, particularly those favoring ammonia volatilization, MgSA consistently supported plant growth across soils, although biomass remained lower in soils A and B compared with soil C. This suggests that the double-salt structure may moderate N losses while still being influenced by soil physicochemical properties. This soil-independent performance reflects the intrinsic stability of the co-crystal, which protects ammonium from rapid loss and releases it gradually as the mineral structure dissolves. Such controlled-release characteristics are highly desirable in lettuce production systems, where rapid early growth requires reliable N availability but where excessive soil nitrate accumulation heightens environmental risks.

Overall, the results show that mechanochemically engineered ammonium-magnesium-sulfate double salts function as efficient, soil-stable nitrogen sources capable of reducing nitrate buildup while sustaining robust early plant growth. The combined plant, soil, and imaging evidence indicate that MgSA improves nitrogen-use efficiency by aligning nutrient release with crop N demand and by mitigating soil-driven loss pathways that limit the performance of conventional fertilizers. These outcomes position mechanochemical co-crystallization as a promising strategy for developing fertilizers that provide both agronomic and environmental benefits, particularly in regions characterized by diverse soil conditions and intensive vegetable production systems.

Although MgSA offers the added advantage of supplying Mg and S as secondary nutrients, repeated application should be optimized according to soil properties and crop demand to avoid potential long-term nutrient imbalance. Future work should evaluate the release kinetics and extractability of N, Mg, and S from MgSA across a broader range of soil pH conditions to better elucidate the mechanisms governing nutrient availability and fertilizer performance in different soil environments.

Conclusions

This work demonstrates how mechanochemical processing can fundamentally reshape the behavior of highly reactive N carriers and transform them into agronomically functional fertilizers. By synthesizing $(NH_4)_2Mg(SO_4)_2 \cdot 6H_2O$ (MgSA), directly AC under dry and wet milling conditions, we show that an unstable, loss-prone ammonium source can be stabilized into a crystalline, nutrient-rich solid without polymer coatings, aqueous processing, or high energy inputs. Structural and surface

analyses, XRD, IR, Raman, and XPS, were used to characterize the physicochemical structure of the resulting double salt, confirming the formation of the unified Mg–NH_4–SO_4 framework in which ammonium is incorporated into a robust solid-state matrix rather than existing as a freely exchangeable ion.

This structural stabilization translated directly into functional improvements. Compared with AC, MgSA exhibited markedly slower nitrogen release, reduced ammonia volatilization, and improved pellet mechanical stability under humid conditions. Nitrogen release kinetics revealed that mechanical co-crystallization effectively dampened the rapid release dynamics that typically drive early-season nitrogen losses. As a result, MgSA behaved not as a simple ammonium salt, but as a controlled-release material whose dissolution and nitrogen availability were governed by solid-state structure rather than solution chemistry alone.

The agronomic implications of this stabilization were evident across three soils spanning a wide range of pH, salinity, and organic matter content. In growth chamber experiments, MgSA consistently supported strong early lettuce growth and canopy development, often matching or exceeding the performance of urea and ammonium carbonate while avoiding excessive soil nitrate accumulation. This cross-soil consistency highlights a key advantage of the double-salt framework: nitrogen delivery was buffered against soil-driven loss pathways, allowing plant uptake to remain reliable even under chemically challenging conditions. The simultaneous supply of magnesium and sulfur further reinforced physiological performance by supporting chlorophyll synthesis and nitrogen assimilation, demonstrating the value of integrating multiple essential nutrients into a single crystalline phase.

Through these efforts, the study demonstrates that magnesium ammonium sulfate double salt can serve as a novel, environmentally friendly, and agronomically valuable controlled-release fertilizer, offering a promising solution for improving nitrogen use efficiency while supplying critical secondary nutrients, sulfur, and magnesium. These findings demonstrate the broader potential of mechanochemistry as a platform for engineering next-generation fertilizers. The favorable agronomic and environmental behavior of MgSA illustrates how solid-state design principles can be leveraged to tune nutrient-release profiles and create fertilizers that simultaneously enhance crop productivity and minimize reactive N accumulation in soils.

Conflicts of interest

There are no conflicts to declare.

Data availability

The data supporting this article have been included as part of the supplementary information (SI). Supplementary information: tables S1–S3. Fresh plant weight (g $plant^{-1}$), ACI, chlorophyll (mg g^{-1} FW), Nitrate (mg kg^{-1} soil) and total nitrogen (mg kg^{-1} soil). See DOI: https://doi.org/10.1039/d6su00101g.

Acknowledgements

The authors acknowledge the non-assistance cooperative agreement between USDA-ARS and Lehigh University under agreement 58-2020-5-051 – USDA and 58-2020-2-013 – USDA. Mention of trade names or commercial products in this publication is solely to provide specific information and does not imply recommendation or endorsement by the USDA. Any opinions, findings, and conclusions, or recommendations expressed in this publication are those of the authors and do not necessarily reflect the views of the USDA. Support for Julia Farias was provided by USDA NACA "Identification of pollutant sources and evaluation of nutrient alternatives for agriculture".

References

1 L. Liu, X. Zhang, W. Xu, X. Liu, Y. Li, J. Wei, M. Gao, J. Bi, X. Lu and Z. Wang, Challenges for global sustainable nitrogen management in agricultural systems, *J. Agric. Food Chem.*, 2020, **68**(11), 3354–3361.
2 N. W. Krase and V. Gaddy, Synthesis of urea from ammonia and carbon dioxide, *Ind. Eng. Chem.*, 1922, **14**(7), 611–615.
3 D. Powlson, Understanding the soil nitrogen cycle, *Soil Use Manage.*, 1993, **9**(3), 86–93.
4 S. Zhou, H. Hou and M. Hosomi, Nitrogen removal, N2O emission, and NH3 volatilization under different water levels in a vertical flow treatment system, *Water Air Soil Pollut.*, 2008, **191**(1), 171–182.
5 A. Mosier, J. Doran and J. Freney, Managing soil denitrification, *J. Soil Water Conserv.*, 2002, **57**(6), 505–512.
6 I. Fillery, J. Simpson and S. De Datta, Contribution of ammonia volatilization to total nitrogen loss after applications of urea to wetland rice fields, *Fert. Res.*, 1986, **8**(3), 193–202.
7 J. Purswani and C. P. Llorente, Nitrification and Denitrification Processes: Environmental Impacts. in *Nitrogen Cycle*, CRC Press, 2021, pp. 60–81.
8 P. S. Selvaraj, K. Periasamy, K. Suganya, K. Ramadass, S. Muthusamy, P. Ramesh, R. Bush, S. G. T. Vincent and T. Palanisami, Novel resources recovery from anaerobic digestates: Current trends and future perspectives, *Crit. Rev. Environ. Sci. Technol.*, 2022, **52**(11), 1915–1999.
9 Đ. Kovačić, Z. Lončarić, J. Jović, D. Samac, B. Popović and M. Tišma, Digestate management and processing practices: a review, *Appl. Sci.*, 2022, **12**(18), 9216.
10 R. Balasubramani, M. K. Awasthi, S. Varjani and N. Karmegam, Aerobic and anaerobic digestion of agro-industrial and livestock wastes: a green and sustainable way toward the future, *Agronomy*, 2023, **13**, 2607.
11 A. Paranjpe, S. Saxena and P. Jain, A review on performance improvement of anaerobic digestion using co-digestion of food waste and sewage sludge, *J. Environ. Manage.*, 2023, **338**, 117733.
12 G. Y. Jayasinghe, T. A. N. T. Perera, W. B. M. A. C. Bandara, K. B. Dassanayake and S. A. D. S. S. Maheepala, A Review of Soil Injection of Liquid Organic Wastes: Potentials and Challenges, *Environ. Process.*, 2022, **9**(2), 37.

13 M. Álvarez Salas, P. Sica, M. Rydgård, T. J. Sitzmann, J. O. Nyang'au, J. El Mahdi, E. Moshkin, H. L. de Castro e Silva, S. Chrysanthopoulos and C. Kopp, Current challenges on the widespread adoption of new bio-based fertilizers: insights to move forward toward more circular food systems, *Front. Sustain. Food Syst.*, 2024, **8**, 1386680.
14 S. Han, S.-i. Jeon, J. Lee, J. Ahn, C. Lee, J. Lee and J. Yoon, Efficient bicarbonate removal and recovery of ammonium bicarbonate as CO2 utilization using flow-electrode capacitive deionization, *Chem. Eng. J.*, 2022, **431**, 134233.
15 A. Moure Abelenda and J. Baltrusaitis, Classical batch distillation of anaerobic digestate to isolate ammonium bicarbonate: Membrane not necessary, *Bioengineering*, 2024, **11**(11), 1152.
16 M. Brondi, R. Bortoletto-Santos, J. G. Farias, C. S. Farinas, M. Ammar, C. Ribeiro, C. Williams and J. Baltrusaitis, Mechanochemically Synthesized Nitrogen-Efficient Mg- and Zn-Ammonium Carbonate Fertilizers, *ACS Sustain. Chem. Eng.*, 2024, **12**(16), 6182–6193, DOI: 10.1021/acssuschemeng.3c07785.
17 L. Su, Y. Ruan, X. Yang, K. Wang, R. Li and Q. Shen, Suppression on plant-parasitic nematodes using a soil fumigation strategy based on ammonium bicarbonate and its effects on the nematode community, *Sci. Rep.*, 2015, **5**(1), 17597.
18 G. Sposito, *The Chemistry of Soils*, Oxford university press, 2008.
19 M. J. Hawkesford and L. J. De Kok, Managing sulphur metabolism in plants, *Plant Cell Environ.*, 2006, **29**(3), 382–395.
20 K. Honer, C. Pico and J. Baltrusaitis, Reactive Mechanosynthesis of Urea Ionic Cocrystal Fertilizer Materials from Abundant Low Solubility Magnesium- and Calcium-Containing Minerals, *ACS Sustain. Chem. Eng.*, 2018, **6**(4), 4680.
21 J. Farias, M. Conley, M. Herritt, C. Call, M. Ammar, M. Eisa, M. Brondi, J. Baltrusaitis, R. Hejl and C. Williams, Assessment of engineered sustainable nitrogen fertilizers on lettuce development using physical sampling and image-based phenotyping, *J. Environ. Qual.*, 2025, **54**, 1397–1415.
22 I. Brekalo, V. Martinez, B. Karadeniz, P. Orešković, D. Drapanauskaite, H. Vriesema, R. Stenekes, M. Etter, I. Dejanović, J. Baltrusaitis, *et al.*, Scale-Up of Agrochemical Urea-Gypsum Cocrystal Synthesis Using Thermally Controlled Mechanochemistry, *ACS Sustain. Chem. Eng.*, 2022, **10**, 6743.
23 D. A. Kosova, A. I. Druzhinina, L. A. Tiflova, A. S. Monayenkova and I. A. Uspenskaya, Thermodynamic properties of ammonium magnesium sulfate hexahydrate (NH4) 2Mg (SO4) 2· 6H2O, *J. Chem. Therm.*, 2018, **118**, 206–214.
24 F. Nadeem, M. A. Hanif, M. I. Majeed and Z. Mushtaq, Role of macronutrients and micronutrients in the growth and development of plants and prevention of deleterious plant diseases-a comprehensive review, *Int. J. Chem. Biochem. Sci.*, 2018, **13**, 31–52.
25 F. J. Maathuis, Physiological functions of mineral macronutrients, *Curr. Opin. Plant Biol.*, 2009, **12**(3), 250–258.
26 H. Marschner, *Marschner's Mineral Nutrition of Higher Plants*, Academic press, 2011.
27 A. Saud, A. Ali and C. A. Quist-Jensen, Magnesium Recovery from Nanofiltration Brine by Membrane Distillation Crystallization, *ACS Sustainable Resour. Manage.*, 2025, **2**(9), 1709–1718.
28 M. Brondi, M. Eisa, R. Bortoletto-Santos, D. Drapanauskaite, T. Reddington, C. Williams, C. Ribeiro and J. Baltrusaitis, Recovering, Stabilizing, and Reusing Nitrogen and Carbon from Nutrient-Containing Liquid Waste as Ammonium Carbonate Fertilizer, *Agriculture*, 2023, **13**(4), 909.
29 M. Govoni Brondi, R. Bortoletto-Santos, J. G. Farias, C. S. Farinas, M. Ammar, C. Ribeiro, C. Williams and J. Baltrusaitis, Mechanochemically Synthesized Nitrogen-Efficient Mg- and Zn-Ammonium Carbonate Fertilizers, *ACS Sustain. Chem. Eng.*, 2024, **12**(16), 6182–6193, DOI: 10.1021/acssuschemeng.3c07785.
30 N. Fairley, V. Fernandez, M. Richard-Plouet, C. Guillot-Deudon, J. Walton, E. Smith, D. Flahaut, M. Greiner, M. Biesinger and S. Tougaard, Systematic and collaborative approach to problem solving using X-ray photoelectron spectroscopy, *Appl. Surf. Sci. Adv.*, 2021, **5**, 100112.
31 J. H. Scofield, Hartree-Slater Subshell Photoionization Cross-Sections at 1254 and 1487 EV, *J. Electron Spectrosc. Relat. Phenom.*, 1976, **8**(2), 129.
32 D. A. Shirley, High-resolution X-ray photoemission spectrum of the valence bands of gold, *Phys. Rev. B*, 1972, **5**(12), 4709.
33 M. Eisa, J. l. G. Farias, M. Ammar, R. Bortoletto-Santos, C. Ribeiro, C. Williams and J. Baltrusaitis, Mechanochemical Synthesis of Nitrogen-Efficient Zn-and Cu-Sulfate Urea Cocrystals from Carbonate Minerals, *ACS Sustainable Resour. Manage.*, 2024, **1**(7), 1363–1376.
34 F. J. Richards, A Flexible Growth Function for Empirical Use, *J. Exp. Bot.*, 1959, **10**(2), 290.
35 F. J. Richards, Plant Physiology: a Treatise, *Analysis of Growth: Behavior of Plants and Their Organs*, 1969.
36 Y. HARA, Application of parametrization using the Richards function to nitrogen release from coated urea and growth of rice seeds, *JARQ (Jpn. Agric. Res. Q.)*, 2001, **35**(3), 155–161.
37 E. Tjørve and K. M. Tjørve, A unified approach to the Richards-model family for use in growth analyses: why we need only two model forms, *J. Theor. Biol.*, 2010, **267**(3), 417–425.
38 D. L. Kerns, M. E. Matheron, J. C. Palumbo, C. A. Sanchez; D. W. Still, B. R. Tickes, K. Umeda and M. A. Wilcox, *Guidelines for head lettuce production in Arizona*, Cooperative Extension, College of Agriculture and Life Sciences, University of Arizona, Tucson, Arizona, IPM Series, 1999, vol. 12.
39 J. Kjeldahl, Neue methode zur bestimmung des stickstoffs in organischen körpern, *Z. für Anal. Chem.*, 1883, **22**(1), 366–382.
40 W. L. Lindsay and W. A. Norvell, Development of a DTPA Soil Test for Zinc, Iron, Manganese, and Copper, *Soil Sci. Soc. Am. J.*, 1978, **42**(3), 421.

41 S. R. Olsen and F. S. Watanabe, A method to determine a phosphorus adsorption maximum of soils as measured by the Langmuir isotherm, *Soil Sci. Soc. Am. J.*, 1957, **21**(2), 144–149.
42 E. E. Schulte and K. Eik, *Recommended Chemical Soil Test Procedures for North Central Region*, 1988.
43 A. Mehlich, Mehlich 3 soil test extractant: A modification of Mehlich 2 extractant, *Commun. Soil Sci. Plant Anal.*, 1984, **15**(12), 1409–1416.
44 G. Bradski, The opencv library, *Dr Dobb's Journal: Software Tools for the Professional Programmer*, 2000, **25**(11), 120–123.
45 S. van der Walt, J. Schönberger, J. Nunez-Iglesias, F. Boulogne, J. Warner, N. Yager, E. Gouillart and T. Yu, scikit-image: image processing in Python, *PeerJ*, 2014, **2**, e453.
46 M. M. Conley, R. W. Hejl, D. D. Serba and C. F. Williams, Visualizing Plant Responses: Novel Insights Possible Through Affordable Imaging Techniques in the Greenhouse, *Sensors*, 2024, **24**(20), 6676.
47 D. E. Karcher and M. D. Richardson, Digital image analysis in turfgrass research, *Turfgrass: Biology, Use, and Management*, 2013, 56, pp. 1133–1149-1132.
48 J. D. Hiscox and G. F. Israelstam, A Method for the Extraction of Chlorophyll from Leaf Tissue without Maceration, *Can. J. Bot.*, 1979, **57**(12), 1332.
49 A. R. Wellburn, The Spectral Determination of Chlorophylls a and b, as Well as Total Carotenoids, Using Various Solvents with Spectrophotometers of Different Resolution, *J. Plant Physiol.*, 1994, **144**(3), 307.
50 F. de Mendiburu and M. F. de Mendiburu, Package 'agricolae', *R Package*, 2019, 1 (3), pp. 1143–1149.
51 E. Erdös, H. Altorfer and J. Witt, Crystal Data for Ammonium Magnesium Carbonate Tetrahydrate [(NH 4) 2 Mg(CO 3) 2 0.4H 2 O], *J. Appl. Crystallogr.*, 1979, **12**(6), 611.
52 B. Li, A. Li, S. Zhao and M. Meyers, Amorphization by mechanical deformation, *Mater. Sci. Eng. R Rep.*, 2022, **149**, 100673.
53 Y. Ma, D. Yuan, B. Mu, L. Gao, X. Zhang and H. Zhang, Synthesis, properties and application of double salt (NH4) 2Mg (SO4) 2· 6H2O in wet magnesium-ammonia FGD process, *Fuel*, 2018, **219**, 12–16.
54 A. Nasser and U. Mingelgrin, Mechanochemistry: A review of surface reactions and environmental applications, *Appl. Clay Sci.*, 2012, **67**, 141–150.
55 Q. Yang, L. Chen, J. Xu, Y. Gong, L. Deng and C. Chen, Study of the corrosion and surface film growth on AZ63 magnesium alloy in MgSO4 solution, *J. Electrochem. Soc.*, 2017, **164**(6), C324.
56 J. Baltrusaitis and V. H. Grassian, Atomic force microscopy and X-ray photoelectron spectroscopy study of NO2 reactions on CaCO3 (1014) surfaces in humid environments, *J. Phys. Chem.*, 2012, **116**(36), 9001–9009.
57 J. S. Stevens, S. J. Byard, C. C. Seaton, G. Sadiq, R. J. Davey and S. L. Schroeder, Proton transfer and hydrogen bonding in the organic solid state: a combined XRD/XPS/ssNMR study of 17 organic acid–base complexes, *Phys. Chem. Chem. Phys.*, 2014, **16**(3), 1150–1160.
58 F. J. Richards, A flexible growth function for empirical use, *J. Exp. Bot.*, 1959, **10**(2), 290–301.
59 F. Richards, The quantitative analysis of growth. Plant physiology, a treatise, Analysis of growth: Behavior of plants and their organs, *Plant Physiol.*, 1968, 3–76.
60 M. Anas, F. Liao, K. K. Verma, M. A. Sarwar, A. Mahmood, Z.-L. Chen, Q. Li, X.-P. Zeng, Y. Liu and Y.-R. Li, Fate of nitrogen in agriculture and environment: agronomic, eco-physiological and molecular approaches to improve nitrogen use efficiency, *Biol. Res.*, 2020, **53**(1), 47.
61 Y. Avnimelech and M. Laher, Ammonia volatilization from soils: Equilibrium considerations, *Soil Sci. Soc. Am. J.*, 1977, **41**(6), 1080–1084.
62 R. Stevens, R. Laughlin and D. Kilpatrick, Soil properties related to the dynamics of ammonia volatilization from urea applied to the surface of acidic soils, *Fert. Res.*, 1989, **20**(1), 1–9.
63 I. Stavi, N. Thevs and S. Priori, Soil salinity and sodicity in drylands: A review of causes, effects, monitoring, and restoration measures, *Front. Environ. Sci.*, 2021, **9**, 712831.
64 A. Otlewska, M. Migliore, K. Dybka-Stępień, A. Manfredini, K. Struszczyk-Świta, R. Napoli, A. Białkowska, L. Canfora and F. Pinzari, When salt meddles between plant, soil, and microorganisms, *Front. Plant Sci.*, 2020, **11**, 553087.
65 S. Ma, G. Wang, S. Su, J. Lu, T. Ren, R. Cong, Z. Lu, Y. Zhang, S. Liao and X. Li, Effects of optimized nitrogen fertilizer management on the yield, nitrogen uptake, and ammonia volatilization of direct-seeded rice, *J. Sci. Food Agric.*, 2023, **103**(9), 4553–4561.
66 K. Dawar, A. Dawar, M. Tariq, I. A. Mian, A. Muhammad, L. Farid, S. Khan, K. Khan, S. Fahad and S. Danish, Enhancing nitrogen use efficiency and yield of maize (Zea mays L.) through Ammonia volatilization mitigation and nitrogen management approaches, *BMC Plant Biol.*, 2024, **24**(1), 74.
67 I. Rorison, The effects of soil acidity on nutrient availability and plant response. in *Effects of Acid Precipitation on Terrestrial Ecosystems*, Springer, 1980, pp. 283–304.
68 F. Adams, Nutritional imbalances and constraints to plant growth on acid soils, *J. Plant Nutr.*, 1981, **4**(2), 81–87.
69 J. Traunfeld, A. Abend and P. Yen, *Lettuce*, 2010.
70 N. D. Adhikari, I. Simko and B. Mou, Phenomic and physiological analysis of salinity effects on lettuce, *Sensors*, 2019, **19**(21), 4814.
71 Z. He, A. Alva, D. Calvert and D. Banks, Ammonia volatilization from different fertilizer sources and effects of temperature and soil pH1, *Soil Sci.*, 1999, **164**(10), 750–758.
72 D. S. Powlson and C. J. Dawson, Use of ammonium sulphate as a sulphur fertilizer: Implications for ammonia volatilization, *Soil Use Manage.*, 2022, **38**(1), 622–634.
73 Y. Li, J. Xu, S. Liu, Z. Qi, H. Wang, Q. Wei, Z. Gu, X. Liu and F. Hameed, Salinity-induced concomitant increases in soil ammonia volatilization and nitrous oxide emission, *Geoderma*, 2020, **361**, 114053.
74 Z.-Q. Shi, D.-L. She, X.-Y. Chen and Y.-Q. Xia, Effects of salinity on soil ammonia volatilization and denitrification rates, *J. Ecol. Rural Environ.*, 2021, **37**(11), 1458–1464.

75 Z. Bie, T. Ito and Y. Shinohara, Effects of sodium sulfate and sodium bicarbonate on the growth, gas exchange and mineral composition of lettuce, *Sci. Hortic.*, 2004, **99**(3–4), 215–224.
76 W. Breś, T. Kleiber, B. Markiewicz, E. Mieloszyk and M. Mieloch, The effect of NaCl stress on the response of lettuce (Lactuca sativa L.), *Agronomy*, 2022, **12**(2), 244.
77 Y. Yang, H. Liu and J. Lv, Evaluation of the applicability of organic amendments from microbially driven carbon and nitrogen transformations, *Sci. Total Environ.*, 2022, **817**, 153020.
78 Q. Chen, Y. Hu, A. Hu, B. Niu, X. Yang, H. Jiao, L. Song and G. Zhang, Shifts in the dynamic mechanisms of soil organic matter transformation with nitrogen addition: From a soil carbon/nitrogen-driven mechanism to a microbe-driven mechanism, *Soil Biol. Biochem.*, 2021, **160**, 108355.
79 A. Gillespie, A. Diochon, B. Ma, M. Morrison, L. Kellman, F. Walley, T. Regier, D. Chevrier, J. Dynes and E. Gregorich, Nitrogen input quality changes the biochemical composition of soil organic matter stabilized in the fine fraction: a long-term study, *Biogeochemistry*, 2014, **117**(2), 337–350.
80 S. Kerley, The effect of soil liming on shoot development, root growth, and cluster root activity of white lupin, *Biol. Fertil. Soils*, 2000, **32**(2), 94–101.
81 M. Borhannuddin Bhuyan, M. Hasanuzzaman, K. Nahar, J. A. Mahmud, K. Parvin, T. F. Bhuiyan and M. Fujita, Plants behavior under soil acidity stress: Insight into morphophysiological, biochemical, and molecular responses, *Plant abiotic stress tolerance: Agronomic, molecular and biotechnological approaches*, 2019, pp. 35–82.
82 L. de Sousa Ferreira, V. de Souza Oliveira, J. J. de Paula Marchiori, T. C. Ferreira, A. C. B. Bernabé, G. T. F. Boone, L. L. dos Santos Pereira and E. Carriço, The nutrient magnesium in soil and plant: a review, *Int. J. Plant Soil Sci.*, 2023, **35**(8), 136–144.
83 N. Ahmed, B. Zhang, B. Bozdar, S. Chachar, M. Rai, J. Li, Y. Li, F. Hayat, Z. Chachar and P. Tu, The power of magnesium: unlocking the potential for increased yield, quality, and stress tolerance of horticultural crops, *Front. Plant Sci.*, 2023, **14**, 1285512.
84 M. Abdallah, L. Dubousset, F. Meuriot, P. Etienne, J. Avice and A. Ourry, Effect of mineral sulphur availability on nitrogen and sulphur uptake and remobilization during the vegetative growth of Brassica napus L, *J. Exp. Bot.*, 2010, **61**(10), 2635–2646.
85 L. J. De Kok, I. Stulen and M. J. Hawkesford, Sulfur nutrition in crop plants, *The Molecular and Physiological Basis of Nutrient Use Efficiency in Crops*, 2011, pp. 295–309.
86 F. Salvagiotti, J. M. Castellarín, D. J. Miralles and H. M. Pedrol, Sulfur fertilization improves nitrogen use efficiency in wheat by increasing nitrogen uptake, *Field Crops Res.*, 2009, **113**(2), 170–177.
87 A. Jamal, Y.-S. Moon and M. Zainul Abdin, Sulphur-a general overview and interaction with nitrogen, *Aust. J. Crop. Sci.*, 2010, **4**(7), 523–529.